HIV-1 Vif disrupts phosphatase feedback regulation at the kinetochore, leading to a pronounced pseudo-metaphase arrest

Dhaval Ghone[1, 2, 6], Edward L. Evans III[1, 3, 5, 6, 8], Madison Bandini[1, 3, 5], Kaelyn G. Stephenson[1], Nathan M. Sherer[1, 4, 5, *], Aussie Suzuki[1, 4, 7, *]

1. McArdle Laboratory for Cancer Research, Department of Oncology, University of Wisconsin-Madison, Madison, Wisconsin, USA
2. Biophysics Graduate Program, University of Wisconsin-Madison, Madison, Wisconsin, USA
3. Cancer Biology Graduate Program, University of Wisconsin-Madison, Madison, Wisconsin, USA
4. Carbone Comprehensive Cancer Center, University of Wisconsin-Madison, Madison, Wisconsin, USA
5. Institute for Molecular Virology, University of Wisconsin-Madison, Madison, Wisconsin 53706, USA
6. These authors contributed equally
7. Lead contact
8. Present address: Laboratory for Optical and Computational Instrumentation, University of Wisconsin-Madison, Madison, Wisconsin, 53705, USA

* Corresponding authors: Aussie Suzuki (aussie.suzuki@wisc.edu) and Nathan Sherer (nsherer@wisc.edu)

Abstract

Virion Infectivity Factor (Vif) of the Human Immunodeficiency Virus type 1 (HIV-1) targets and degrades cellular APOBEC3 proteins, key regulators of intrinsic and innate antiretroviral immune responses, thereby facilitating HIV-1 infection. While Vif's role in degrading APOBEC3G is well-studied, Vif is also known to cause cell cycle arrest, but the detailed nature of Vif's effects on the cell cycle has yet to be delineated. In this study, we employed high-temporal single-cell live imaging and super-resolution microscopy to monitor individual cells during Vif-induced cell cycle arrest. Our findings reveal that Vif does not affect the G2/M boundary as previously thought. Instead, Vif triggers a unique and robust pseudo-metaphase arrest, distinct from the mild prometaphase arrest induced by Vpr. During this arrest, chromosomes align properly and form the metaphase plate, but later lose alignment, resulting in polar chromosomes. Notably, Vif, unlike Vpr, significantly reduces the levels of both Protein Phosphatase 1 (PP1) and 2A (PP2A) at kinetochores, which regulate chromosome-microtubule interactions. These results unveil a novel role for Vif in kinetochore regulation that governs the spatial organization of chromosomes during mitosis.

55 **Introduction**

56 The human immunodeficiency virus type 1 (HIV-1) weakens the immune system by
57 depleting CD4+ T cells, eventually causing the Acquired Immunodeficiency Syndrome (AIDS)
58 (Deeks et al, 2015; Swanstrom & Coffin, 2012). As a result, HIV-1 infected individuals have an
59 increased susceptibility to specific cancers and other health complications (Cohen et al, 2016;
60 Grulich et al, 2007; Hernández-Ramírez et al, 2017; Parkin, 2006). After HIV-1 enters a host cell,
61 its RNA genome undergoes reverse transcription to form double-stranded DNA, followed by
62 integration of the DNA provirus into the host's genome. Using the host's transcriptional
63 machinery, HIV-1 transcribes its genome into spliced, partially spliced and completely unspliced
64 viral mRNAs, facilitating viral gene expression and infectious virion production (Jouvenet et al,
65 2009; Nguyen & Hildreth, 2000; Ono & Freed, 2001). While the mechanisms underlying CD4+ T
66 cell depletion during HIV-1 infection remain an active area of research, evidence suggests that
67 both direct cytopathic effects of HIV-1 and chronic hyperactivation of the immune system
68 contribute significantly. These processes drive apoptosis and induce pyroptosis in CD4+ T cells,
69 leading to their progressive loss (Doitsh & Greene, 2016; Vidya Vijayan *et al*, 2017).

70 HIV-1 encodes four accessory viral proteins (Vif, Vpr, Vpu, and Nef) that are nonessential
71 for virus replication in some ex vivo cell culture systems (Gabuzda et al, 1992) but play crucial
72 immunomodulatory roles in vivo (Malim & Emerman, 2008). The primary role of Vif (Virion

73 Infectivity Factor) is to facilitate the proteasomal degradation of APOBEC3 (A3) family of cytidine
74 deaminases (e.g., A3F, A3G, and A3H). A3 proteins introduce deleterious mutations into the HIV-
75 1 genome by deaminating cytosine residues in the viral single-stranded DNA during reverse-
76 transcription, converting them to uracil (Chiu & Greene, 2009; Okada & Iwatani, 2016). Vif
77 orchestrates A3 protein degradation by recruiting an E3 ubiquitin ligase complex (Conticello et
78 al, 2003; Marin et al, 2003; Sheehy et al, 2003; Stopak et al, 2003; Yu et al, 2003). This
79 degradation prevents A3 proteins from being incorporated into budding viral particles, ensuring
80 that the progeny virions remain infectious.

81 Independently of its primary role of A3 protein degradation (DeHart et al, 2008; Du et al,
82 2019; Zhao et al, 2015), several studies have shown Vif to induce cell cycle arrest and cell death
83 in CD4+ T cells and several other cell types (DeHart et al., 2008; Du et al., 2019; Greenwood et
84 al, 2016; Marelli et al, 2020; Nagata et al, 2020; Sakai et al, 2006; Salamango et al, 2019; Zhao
85 et al., 2015). However, the molecular mechanisms that underpin these effects remain unclear. A
86 prior study indicated that p53, a tumor suppressor, is required for Vif-induced G2/M cell cycle
87 arrest (Izumi et al, 2010). Several recent studies suggest that Vif's cell cycle arrest activity is due
88 to the loss of B56 proteins that are regulatory subunits of protein phosphatase 2A (PP2A)
89 (DeHart et al., 2008; Du et al., 2019; Greenwood et al., 2016; Marelli et al., 2020; Nagata et al.,
90 2020; Salamango et al., 2019; Salamango et al, 2020; Zhao et al., 2015). The PP2A-B56

91 complex is a serine-threonine protein phosphatase that participates in various key G2 and mitotic
92 processes (Lee et al, 2017; Schuhmacher et al, 2019). Additionally, earlier research has
93 demonstrated that Vif can lead to reductions in Cyclin F (Augustine et al, 2017), a non-canonical
94 cyclin critical for late S- and G2-phase progression (Clijsters et al, 2019; Enrico et al, 2021), or
95 affect both Cdk1 and Cyclin B1, which are essential for the transition into and out of mitosis
96 (Sakai et al, 2011).

97 These prior studies have predominantly employed flow cytometry-based techniques to
98 measure cell cycle phase population densities. However, flow cytometry has limitations in its
99 ability to differentiate between late S, G2, and M phases, because it categorizes cell cycle
100 phases solely based on relative DNA content. Accordingly, in this study we prioritized high-
101 temporal single-cell live imaging that would allow us to directly observe the disruptions of cell
102 cycle triggered by Vif expression. We demonstrate that Vif induces a highly unique and robust
103 pseudo-metaphase arrest, irrespective of cell line tested or p53 status. Additionally, we found
104 that Vpr unexpectedly induces a distinct mitotic delay, clearly different from the pseudo-
105 metaphase arrest caused by Vif. Vif, but not Vpr, disrupts the localizations of PP2A-B56 at the
106 kinetochores during prometaphase, leading to a slight yet significant delay in the alignment of
107 chromosome at metaphase. This disruption results in reduced localization of the Astrin-SKAP-
108 PP1 complex at the kinetochores, causing improper kinetochore-microtubule binding affinity due

to increased phosphorylation of the microtubule binding protein at kinetochores. These effects yield unbalanced forces between sister chromatids, resulting in misaligned chromosomes and abnormal chromosomal movements in association with spindle microtubules. These insights provide a deeper understanding of Vif's impact on the regulation of the host cell cycle, a conserved feature of Vif that may have potential relevance to HIV-1 pathogenesis in vivo.

127 **Results**

128 **Vif and Vpr induce distinct forms of mitotic arrest**

129 Previous research demonstrated that both Vif and Vpr expression causes cell cycle arrest and
130 cytotoxicity in CD4+ T cells and as well as many cancer cell lines (Augustine *et al.*, 2017;
131 Emerman, 1996; Evans *et al*, 2018; Nagata *et al.*, 2020; Sakai *et al.*, 2011; Sakai *et al.*, 2006;
132 Salamango *et al.*, 2019; Salamango *et al.*, 2020; Wang *et al*, 2011; Wang *et al*, 2008). To
133 investigate the nature of the cell cycle arrest induced by Vif, we employed high-temporal live cell
134 imaging using the triple negative breast cancer Cal51 cell line. This cell line was chosen for
135 several reasons; it has been engineered for precise cell cycle tracking through CRISPR-Cas9-
136 mediated endogenous tagging of Histone H2B with mScarlet, allowing visualization of DNA, and
137 Tubulin with mNeonGreen, to enable monitoring the microtubule cytoskeleton (Scribano et al,
138 2021). This approach minimizes the confounding effects of exogenous overexpression of
139 fluorescently labeled Histone and Tubulin proteins on cell cycle progression (**Fig 1A**). Moreover,
140 Cal51 cells are well-suited for long-term live cell imaging assays due to their adherent growth
141 properties, which facilitate extended single-cell monitoring. They also exhibit a stable, near-
142 diploid karyotype and retain wild-type p53 expression, making them an ideal model for cell cycle
143 research (Lynch et al, 2022). For these experiments, we infected cells with the NL4-3 strain HIV-
144 1 reporter viruses expressing either Vif (“Vif”), Vpr (“Vpr”), a combination of both (“Vif+Vpr”), or

145 a lack of both (“Control”) (**Fig S1A**) (Evans *et al.*, 2018). Note that the NL4-3 strain encodes all
146 known HIV-1 proteins and serves as a well-established model for studying various aspects of
147 HIV-1 biology (Mustafa & Robinson, 1993). These reporter viruses contain cyan fluorescent
148 protein (CFP), allowing us to identify infected cells under fluorescence microscopy. To focus our
149 study on the effects of these proteins on the cell cycle, the reporter viruses do not express the
150 viral Env and Nef proteins, which are known to exhibit cytotoxicity (Elder, 2002; Emerman, 1996;
151 Evans *et al.*, 2018).

152 We then assessed the mitotic duration defined as the time between nuclear envelope
153 breakdown (NEBD) and anaphase onset in CFP-positive cells using video microscopy. Vif-
154 expressing Cal51 cells demonstrated a prolonged mitosis of ~16 hours, in contrast to only 30
155 min in Control cells (**Fig 1B and Movies S1-2**). Great majority of Vif-expressing cells eventually
156 succumbed to apoptotic cell death or exhibited mitotic slippage, wherein the cell exited mitosis
157 without completing chromosome segregation (**Fig 1C and S1B**).

158 Vpr has been known to induce G2/M arrest in a variety of cell types, as evidenced by
159 flowcytometry (Bartz *et al*, 1996; Elder, 2002; Emerman, 1996; Hall *et al*, 2024; He *et al*, 1995;
160 Jowett *et al*, 1995; Sakai *et al.*, 2006). We next examined the differences in G2/M arrests induced
161 by Vif and Vpr. While we expected Vpr to induce G2 phase arrest due to its abilities to cause
162 DNA damage, our live-cell imaging revealed that Vpr-expressing cells also experienced a

163 prolonged mitosis of ~1.7 hours, which is significantly shorter than in Vif-expressing cells (**Fig**
164 **1A-B**). Interestingly, Vif+Vpr-expressing cells exhibited a prolonged mitosis lasting ~21.7 hours,
165 indicating that Vif plays a dominant role in mitotic arrest when both proteins are present.
166 Supporting this, the majority of Vif-expressing or Vif+Vpr-expressing mitotic cells underwent
167 apoptotic cell death, whereas Vpr-expressing mitotic cells either completed division or
168 experienced mitotic slippage. In summary, although both Vif and Vpr can induce a prolonged
169 mitosis, Vif causes significantly more severe mitotic arrest, leading to cell death.

170 To pinpoint the specific sub-stage of mitosis affected by Vif expression, we closely
171 assessed chromosome alignment during metaphase. Notably, most Vif-expressing Cal51 cells
172 successfully achieved metaphase chromosome alignment (metaphase plate) similar to the
173 control cells, but with a slight delay, reaching it approximately 1.5 hours post-NEBD compared
174 to the control's ~30 minutes. (**Fig 2A-C**). However, this alignment was unstable and deteriorated
175 over time in Vif-expressing cells. Mitotic arrest induced by common mitotic inhibitors is seen in
176 prometaphase before achieving the metaphase plate (Choi et al, 2011). However, the mitotic
177 arrest caused by Vif was distinctive because cells were able to complete prometaphase but then
178 gradually lost proper chromosome spatial organization at the metaphase plate over time.
179 Accordingly, we termed this block “pseudo-metaphase arrest”. Consistent with our findings in
180 Cal51 cells, other commonly used cell lines for cell cycle studies, such as HeLa and MDA-MB-

181 231, also demonstrated significant mitotic arrest (approximately 12 hours for both) following Vif
182 expression, which subsequently led to either apoptotic cell death or mitotic slippage (**Fig S1C-E**
183 **and S2A-C**). Similar to Cal51, the majority of these Vif-expressing cells were able to establish a
184 metaphase plate early but were unable to enter anaphase (**Fig S1F-G and S2D-E**). Consistent
185 with these results, Vif-expressing HeLa cells exhibited a markedly higher mitotic index compared
186 to Control cells at 72 hours post-infection in fixed immunofluorescence (IF) (**Fig S1H**). In
187 conclusion, Vif triggers a marked pseudo-metaphase arrest in a range of cell lines. Most of these
188 arrested cells experienced either apoptotic cell death or mitotic slippage, suggesting a conserved
189 underlying mechanism.
190

191 **Solo Vif expression is sufficient to trigger a robust pseudo-metaphase arrest**

192 To determine if Vif expression alone is sufficient to induce a robust pseudo-metaphase
193 arrest in the absence of other viral factors, we next engineered HeLa cells to conditionally
194 express codon optimized Vif (CO-Vif) under the control of a doxycycline-inducible promoter (Das
195 et al, 2016). As a control, we employed the same system but with mNeonGreen expression
196 instead of Vif. Control cells displayed mNeonGreen signals approximately 10 hours post-
197 doxycycline induction. In line with these expression kinetics, cells expressing CO-Vif almost
198 invariably exhibited pseudo-metaphase arrest roughly 10 hours post-induction; with cells

199 arrested for ~15h in contrast to Control cells that proceeded through mitosis in ~1 hour (**Fig 2D-**
200 **E and Movies S3-4**). While Control cells continued to propagate, those expressing Vif did not,
201 with Vif expression alone confirmed as sufficient to trigger prolonged pseudo-metaphase arrest
202 and apoptotic cell death (**Fig 2F-G**).
203
204 **Vif accelerates G2 progression with no effect on the G1 or S phases**
205 We next asked if Vif altered other stages of the cell cycle in addition to mitosis. To this end, we
206 developed a novel method that allowed us to accurately distinguish between G1, S, and G2
207 phases in individual Cal51 reporter cells during live cell imaging based on tracking changes to
208 the intensity of Histone H2B-mScarlet over time (see **Methods**). This method offers the
209 advantage of allowing us to measure temporal changes of the DNA content at single cell
210 resolution with high accuracy. Briefly, during S phase, H2B-mScarlet signals increased steadily,
211 eventually plateauing and remaining constant throughout the G2 phase. **Fig 3A** presents
212 example images and an intensity profile covering the period from the end of one mitosis to the
213 beginning of the next in a Control Cal51 cell. Using this method, we observed no significant
214 differences in the durations of either G1 or S phases in both Control or Vif-expressing cells.
215 However, Vif-expressing cells exhibited a slight yet statistically significant reduction in G2 phase
216 duration compared to Control cells (**Fig 3B-C and S3A**). Consistent to Cal51 cells, Vif expression

217 also did not significantly impact the duration of interphase in two additional cell lines, RPE1 and
218 MDA-MB-231 cells (**Fig. S3B).** In summary, these findings demonstrated that Vif expression
219 induces pseudo-metaphase arrest without notably affecting the overall duration of interphase
220 (the cumulative time of G1, S, and G2 phases).
221

222 **Vif Induces Pseudo-Metaphase Arrest Independently of p53**

223 A previous study indicated that Vif-induced cell cycle arrest is due to tumor suppressor p53
224 (Izumi et al., 2010), which is well established to trigger G2 cell cycle arrest in response to DNA
225 damage (St Clair et al, 2004; Stark & Taylor, 2006; Taylor & Stark, 2001). Considering that we
226 had already observed Vif inducing pseudo-metaphase arrest in cell lines with functionally
227 inactivated p53, such as HeLa (Evans et al., 2018; Wang et al., 2011) and MDA-MB-231 (Olivier
228 et al, 2002) (**Fig S1C-D and S2A-B**), we further investigated the potential p53-dependency by
229 assessing Vif's effects in p53 null knockout (p53 KO) RPE1 (Mardin et al, 2015) or HCT116 cell
230 lines (**Fig 3D-G**). Both wild-type (p53 +/+) and p53 KO RPE1 and HCT116 cells demonstrated
231 significant pseudo-metaphase arrest in response to viral Vif expression. Specifically, RPE1 wild-
232 type cells were arrested for >10 hours, RPE1 p53 KO cells for ~25 hours, and both HCT116 wild-
233 type and p53 KO cells for >6 hours. In contrast, cells infected with the Vif-negative Control virus
234 showed no delay in mitosis (~30 min for both cell lines) (**Fig 3D-E and S3D-E**). All cell lines,

235 regardless of p53 status, managed to establish a chromosome metaphase plate in the presence
236 of Vif expression (**Fig 3F-G and S3F-G**). However, most Vif-expressing cells exhibited apoptotic
237 cell death or mitotic slippage (**Fig S3C and S3H**).
238

239 **Vif-induced pseudo-metaphase arrest disrupts spatial organization of chromosomes and**
240 **spindle poles**

241 To further characterize the mitotic defects caused by Vif expression, we carefully
242 assessed Vif's effects on chromosome alignment at the metaphase plate. To this end, we
243 employed super-resolution microscopy and stained for CENP-C, microtubules, and DNA (see
244 **Methods**). CENP-C is a marker for kinetochores, the platform for microtubule attachment on
245 mitotic chromosomes. Our findings revealed that ~100% of Vif-expressing mitotic cells exhibited
246 misaligned chromosomes, with the great majority of these misaligned chromosomes
247 concentrated at spindle poles as polar chromosomes (**Fig 4A-B, S4A, and Movies S5-6**).

248 We next explored the dynamics of chromosome spatial organization in Vif-expressing
249 cells by using live cell imaging. To do this, we first quantified the proportion of cells exhibiting
250 polar chromosomes at any time point during metaphase/pseudo-metaphase for all four of our
251 cell systems (HeLa, RPE1, MDA-MB-231, and Cal51 cells). Consistent with our fixed-cell
252 analysis, we observed ~100% of Vif-expressing cells exhibiting misaligned polar chromosomes

253 at some time point during the prolonged mitosis, in contrast to Control cells in which misaligned
254 chromosomes were only rarely observed (**Fig S4B**). To define the dynamic nature of
255 chromosome movements, we segmented cells into two compartments, polar and equatorial, and
256 then measured the Histone H2B-mScarlet signals within each of these compartments in Cal51
257 cells over time (**Fig 4C**). Vif-expressing cells exhibited an initial decrease in the frequency of
258 polar chromosomes shortly after NEBD, but this frequency increased significantly during the
259 extended pseudo-metaphase; with pronounced polar chromosomes comprising ~50% of the
260 total DNA. Notably, these misaligned chromosomes continuously oscillated between the poles
261 and the metaphase plate, as shown in **Fig 4D**.

262 Consistent with abnormal chromosome dynamics, ~25% of HeLa cells expressing Vif
263 exhibited multi-polar spindles (>2 poles) at 72h post-infection based on fixed cell analysis (**Fig**
264 **S4C**). To corroborate these findings, we used high-temporal live cell imaging to track and
265 quantify spindle poles using mNeonGreen-Tubulin in Cal51 cells. We observed that ~80% of
266 cells expressing Vif demonstrated multi-polarity at some time point during the extended mitosis.
267 Moreover, the number of spindle poles varied dramatically in arrested cells, ranging from a
268 monopole to as many as five poles (**Fig 4E and S4D**).

269 The integrity of spindle poles is crucial for maintaining the position of the metaphase
270 plate during mitotic progression, so that the length of microtubules making up the mitotic spindle

271 is tightly regulated and typically remains stable until anaphase onset. Interestingly, we found that
272 mitotic spindles in Vif-expressing cells were significantly stretched (~18 μm in length) as
273 compared to Control cells (~12 μm) (**Fig 4F and S4E**). Moreover, although mitotic spindles are
274 typically stationary, we observed spindles in Vif-expressing cells to exhibit dynamic spinning. To
275 define these observations quantitatively, we measured the average angle swept by individual
276 mitotic spindles over time in the presence or absence of Vif expression, observing a greater than
277 15-fold increase in the angle covered by spindles in Vif-expressing cells as compared to Control
278 cells (**Fig 4G and S4F**). In summary, Vif induces dynamic movements in both chromosomes and
279 spindle poles during extended pseudo-metaphase, resulting in severely misaligned polar
280 chromosomes.
281

282 **Vif, but not Vpr, disrupts the proper localization of PP2A-B56 at the kinetochores**

283 Microtubule assembly at the kinetochore is regulated by an intricate network of kinase
284 and phosphatases (Saurin, 2018). PP2A-B56 is recruited to kinetochores during prometaphase,
285 where it plays a crucial role in microtubule assembly and the proper alignment of chromosomes
286 (Foley & Kapoor, 2013; Foley *et al*, 2011). Previous studies demonstrated that Vif can
287 significantly degrade B56 proteins, as shown by western blots (Greenwood *et al.*, 2016; Marelli
288 *et al.*, 2020; Nagata *et al.*, 2020). Therefore, we investigated whether Vif-expressing mitotic cells

289 had diminished B56 at kinetochores. To address this, we performed quantitative
290 immunofluorescence (qIF) using specific antibodies against B56 and CENP-C (as a kinetochore
291 marker) in Control, Vif-expressing, and Vpr-expressing cells. We found that B56 signals at
292 kinetochores, regardless of aligned (equatorial) or unaligned (polar) chromosomes, were
293 significantly reduced in Vif-expressing cells compared to Control and Vpr-expressing cells (**Fig**
294 **5A-C**). To determine whether Vif-expressing cells remained free of additional, non-kinetochore-
295 bound pools of B56, we performed qIF in nocodazole treated cells. It has been demonstrated
296 that nocodazole, microtubule depolymerizer, can enhance B56 kinetochore localization (Foley
297 *et al.*, 2011). As expected, Control cells showed further recruitment of B56 to kinetochores upon
298 nocodazole treatment, whereas Vif-expressing cells did not (**Fig 5A and 5C**). These results
299 suggest that Vif-mediated degradation of B56 is sufficient to significantly reduce B56 levels at
300 kinetochores during prometaphase, while Vpr has no effect on B56 levels at kinetochores. To
301 further validate these results, we performed qIF on Polo-like Kinase 1 (Plk1). Plk1 is a key cell
302 cycle regulator with critical roles at kinetochores in proper mitotic progression (Colicino & Hehnly,
303 2018). It is known that Plk1 levels at kinetochores are regulated by PP2A-B56, and depletion of
304 B56 causes increased levels of Plk1 at kinetochores, leading to improper microtubule
305 attachments (Foley *et al.*, 2011). As expected, Plk1 levels at kinetochores were significantly
306 dropped in metaphase as compared to prometaphase in Control cells (**Fig 5D-E**). In Vif-

307 expressing cells, while Plk1 levels at kinetochores in equatorial chromosomes were lower than
308 those on polar chromosomes, Vif-expressing cells showed a global increase in Plk1 levels at
309 kinetochores. More specifically, Plk1 levels at polar chromosomes in Vif-expressing cells were
310 significantly higher than in Control prometaphase, and levels at aligned equatorial chromosomes
311 were also significantly higher than in Control metaphase. In summary, Vif, but not Vpr,
312 significantly diminishes PP2A-B56 levels at kinetochores, resulting in a delay of chromosome
313 alignments.
314

315 **Vif impairs stable and balanced kinetochore microtubule attachments**

316 We demonstrated that Vif-expressing cells exhibited abnormal dynamic chromosome
317 movements (**Fig 4D-G**). Kinetochore-microtubule bindings are stabilized by both PP2-B56 and
318 PP1 at kinetochores through an interplay and feedback mechanism (Saurin, 2018; Vallardi *et al*,
319 2017). Consequently, we hypothesized that the reduction of PP2A-B56 by Vif impaired the
320 regulation PP1 phosphatase activities at kinetochores. To test this hypothesis, we quantified the
321 levels of the Astrin-SKAP complex (hereinafter referred to as 'Astrin') at kinetochores by qIF in
322 HeLa cells in the presence or absence of Vif expression. Astrin stabilizes kinetochore-
323 microtubule attachments by recruiting PP1, which dephosphorylates Hec1, a microtubule
324 binding protein at kinetochores, thereby promoting Hec1 binding to microtubules (Cheeseman

325 *et al*, 2006; Conti *et al*, 2019; Dunsch *et al*, 2011; Manning *et al*, 2010; Schmidt *et al*, 2010;
326 Zhang *et al*, 2015). As expected, Astrin signals at kinetochores significantly increased at
327 metaphase compared to prometaphase in Control cells (**Fig 6A-B**). In contrast, Astrin levels at
328 kinetochores on aligned chromosomes (equatorial) in Vif-expressing cells were approximately
329 50% of control, and Astrin levels on polar chromosomes largely undetectable (**Fig 6A-B**). We
330 confirmed that levels of CENP-C, which is a core-structural kinetochore protein, did not change
331 between Control and Vif-expressing cells, indicating that the reduction of Astrin in Vif-expressing
332 cells was not due to compromised kinetochore integrity (**Fig 6A-B**).

333 Generating uniform pulling force across sister kinetochores is essential for maintaining
334 chromosome alignment at the cell equator during metaphase. While control cells showed equal
335 Astrin recruitment at sister kinetochores, consistent with balanced forces (**Fig 6C)**, Vif-
336 expressing cells showed significant differences in Astrin levels between sister kinetochores
337 despite CENP-C levels remaining consistent (**Fig 6B-C)**.

338 The N-terminal domain of Hec1 has multiple phosphorylation sites, and
339 dephosphorylation specifically by PP1 is critical for stabilizing its binding to microtubules
340 (DeLuca *et al*, 2011). To directly validate the reduced activity of PP1 at kinetochores in Vif-
341 expressing cells, we performed qIF using a phospho-Hec1 S55 antibody (pS55). As expected,
342 phosphorylation levels pS55 were high in Control prometaphase and significantly reduced in

343 metaphase (**Fig 6D-E**). In contrast, pS55 levels remained significantly high at aligned
344 chromosomes (equatorial) in Vif-expressing cells compared to aligned metaphase
345 chromosomes in Control cells (**Fig 6D-E**). Similarly, unaligned chromosomes (Polar) maintained
346 pS55 levels similar to those in Control prometaphase. We confirmed that Hec1 levels at
347 kinetochores were the same in both Vif-expressing and Control cells (**Fig 6G-H**). These results
348 demonstrate that PP1 activity at kinetochores is weaker in Vif-expressing cells compared to
349 Control cells. In agreement with the unbalanced Astrin recruitment at sister kinetochores in Vif-
350 expressing cells, pS55 levels between sister kinetochores were also significantly unbalanced in
351 Vif-expressing cells compared to Control cells (**Fig 6F**). In summary, Vif disrupts the proper
352 assembly of the Astrin-PP1 complex at kinetochores, resulting in the retention of high
353 phosphorylation Hec1 levels. This leads to weakened and uneven forces between sister
354 kinetochores, likely contributing to dynamic chromosome movements.
355

356 **Limitations of the study**

357 To study the spatiotemporal regulation of Vif and the effects of its expression levels at
358 the single-cell level, we aimed to visualize Vif's trafficking during the cell cycle. We discovered
359 that C-terminal fusion of tags, such as 3xHA or mCherry, abolishes Vif's ability to induce pseudo-
360 metaphase arrest (**Fig S5A-E**). In this study, we elucidate the mechanisms underlying Vif-

361 induced pseudo-metaphase arrest by utilizing cancer cell lines and a non-transformed normal
362 cell line. While performing similar high-temporal resolution long-term imaging on well-established
363 host cell types for HIV-1 (primary CD4+ T cells, lymphocytes, dendritic cells, or macrophages)
364 poses significant technical challenges, future studies are required to investigate these cell types.
365 Such investigations will help determine whether Vif can contribute to the suppression of the host
366 immune system by effectively induce robust pseudo-metaphase arrest, ultimately leading to cell
367 death.
368
369
370 **Discussion**
371 The specific processes by which HIV-1 causes loss of CD4+ T cells are numerous and
372 include activation of innate immune sensors (Doitsh & Greene, 2016), Envelope-driven cell
373 fusion/syncytiation (Nardacci et al, 2015), and induction of cell cycle arrest followed by
374 programmed cell death mediated by viral gene products that include Vif and Vpr (Muthumani et
375 al, 2005). Vif has recently been shown to induce cell cycle arrest in conjunction with its
376 downregulation of PP2A-B56 subunits (Marelli et al., 2020; Nagata et al., 2020; Salamango et
377 al., 2019). However, the specific nature of this arrest was not previously examined at the level
378 of single cells and had been assumed to occur during G2 based on flow cytometric assays. In

379 our study, we discovered that expression of Vif actually reduces the duration of G2 (**Fig 3B**) and
380 instead triggers a robust pseudo-metaphase arrest, confirmed in a broad range of cell lines, and
381 with cells typically succumbing to apoptotic cell death after extended pseudo-metaphase (**Fig**
382 **1C, 1H, S1E, S2C**). We also demonstrate that, contrary to a prior study (Izumi et al., 2010), Vif-
383 induced pseudo-metaphase arrest occurs independently of p53 status (**Fig 3D-F and S3D-F**).

384 Further, we demonstrate that Vif specifically disrupts the kinetochore functions, impairing
385 proper mitotic progression (**Fig. 6A-B)**. Normally, after NEBD, microtubules efficiently capture
386 kinetochores during prometaphase through the interplay of PP1 and PP2A-B56 phosphatase
387 activities (Sivakumar & Gorbsky, 2017; Smith *et al*, 2019; Vallardi *et al.*, 2017). PP2A-B56 is
388 recruited to kinetochores in prometaphase, reducing Plk1 activity to facilitate kinetochore-
389 microtubule assembly and promoting recruitment of PP1 by multiple adaptors. A major PP1
390 adaptor for kinetochore recruitment is the Astrin-SKAP complex whose recruitment requires
391 proper microtubule end-on attachment (Conti *et al.*, 2019; Friese *et al*, 2016; McVey *et al*, 2021).
392 In Vif-expressing cells, Vif significantly reduces the level of PP2A-B56 at kinetochore in
393 prometaphase, likely due to its role in B56 degradation. This reduction leads to a slower
394 establishment of metaphase plate (**Fig 7**). The significant loss of PP2A-B56 at kinetochores
395 impairs the feedback control necessary for stabilizing microtubule binding. As a result, there is
396 a significantly lower and uneven recruitment of Astrin-SKAP-PP1 complex to kinetochores,

397 causing uneven pulling forces between sister chromatids that result in some chromosomes being
398 prematurely pulled towards spindle poles prior to satisfying the mitotic checkpoint (**Fig 7D, Step**
399 **1**). Upon approaching the spindle poles, Aurora A, another key kinase that regulates mitotic error
400 correction, phosphorylates the MTBDs of Ndc80/Hec1 and destabilizes kinetochore-microtubule
401 attachment (**Fig 7D, Step 2**) (Anna *et al*, 2015; Barr & Gergely, 2007; Chmátal *et al*, 2015;
402 DeLuca, 2017; DeLuca *et al.*, 2011; Kettenbach *et al*, 2011). This destabilization of the
403 kinetochore-microtubule attachment could explain why polar chromosomes in Vif-expressing
404 cells lose Astrin signals at kinetochores (**Fig 6A-B**). Polar chromosomes are then transported
405 back to the equator by polar-ejection forces (**Fig 7D, Step 3**) (Poser et al, 2019; Wandke et al,
406 2012). The repetition of this cycle accounts for the observed abnormal dynamics of chromosome
407 movements in Vif-expressing cells.
408
409
410 **Acknowledgement**
411 We would like to thank YuHi Hara, Takanori Tsuchiya, Yokogawa Corporation, Nikon, and Tokai
412 Hit for critical equipment and technical support. We also would like to thank Dr. James Bruce for
413 the critical suggestions and experimental support and Ms. Ainslie Homan for support in data
414 analysis. Part of this work is supported by the University of Wisconsin-Madison Office of the Vice

Chancellor for Research with funding from the Wisconsin Alumni Research Foundation, start-up funding from University of Wisconsin-Madison SMPH, UW Carbone Cancer Center, and McArdle Laboratory for Cancer Research, and NIH grant R35GM147525 and U54AI170660 (to A.S.) and U54AI170660, R01AI110221, and P01CA022443 (to N.S.).

Author contribution

E.L.E. III initiated the project, identified Vif-induced metaphase arrest, and generated key viral reagents and NL4-3 strain HIV-1 reporter vectors. D.G. conducted the bulk of the follow-up precision imaging experiments and analyses, with assistance from M.B., K.G.S., N.S., and A.S.. A.S. and N.S. conceptualized, supervised and funded the project. D.G. and A.S. prepared the initial manuscript draft, with assistance from N.S., E.L.E. III, and M.B. All authors reviewed and contributed to the manuscript's refinement.

Competing Financial Interests

The authors declare no further conflict of interests.

Methods

Cell Culture

433 Human HeLa, RPE1, Cal51, and MDA-MB-231 cells were originally obtained from the American
434 Type Culture Collection (ATCC, Manassas, VA, USA). RPE1 p53 KO, HCT116 p53 KO, RPE1
435 (H2B-RFP), MDA-MB-231 (H2B-mCherry), and Cal51 (Tubulin-mNeonGreen and H2B-mScarlet
436 were endogenously tagged by CRISPR-Cas9) cells were originally obtained from Dr. Jan Korbel,
437 Dr. Yue Xiong (UNC), Dr. Mark Burkard, and Dr. Beth Weaver, respectively. H2B-GFP expressing
438 HeLa cells and conditional CO-Vif-expressing HeLa cells using a pCEP4 vector (Thermo)
439 containing the TRE and Tet promotor with codon-optimized Vif or mNeonGreen were generated
440 in this study. HeLa, MDA-MB-231, HCT116, RPE1 and Cal51 were grown in DMEM high glucose
441 (Cytiva Hyclone; SH 30243.01) or DMEM/F12 (Cytiva Hyclone; SH 3026101) supplemented with
442 1% penicillin-streptomycin, 1% L-glutamine, and 10% fetal bovine serum under 5% CO_2 at 37ºC
443 in an incubator.
444

445 **Live cell imaging**

446 RPE1, Cal51, HeLa, and MDA-MB-231 cells were plated on 4-chamber 35mm glass bottom
447 dishes at least one day prior to imaging (4 chamber with #1.5 glass, Cellvis). In a subset of
448 experiments, cells were stained using sirDNA (Cytoskeleton, 150 nM) for 2 hours prior to imaging
449 to visualize chromosomal DNA. For conditionally Vif-expressing cells, doxycycline (1 µg/ml,
450 Sigma) was supplemented prior to imaging. High temporal resolution live-cell imaging was

451 performed using a Nikon Ti2 inverted microscope equipped with a Hamamatsu Fusion camera,
452 spectra-X LED light source (Lumencor), Shiraito PureBox (TokaiHit), and a Plan Apo 20x
453 objective (NA = 0.75) controlled by Nikon Elements software. Cells were recorded at 37°C with
454 5% CO2 in a stage-top incubator using the feedback control function to accurately maintain
455 temperature of growth medium (Tokai Hit, STX model). Images were recorded for 48-120 hours
456 at 6-12 min intervals with three to four z-stack images acquired at steps of 1.5~2 μm for each
457 time point.
458

459 **Fixed high- and super-resolution imaging**

460 HeLa cells infected "Control" (Vif-negative) and Vif-containing viruses were fixed by 4% PFA
461 (Sigma) at 72 hours post-infection. Cells were then permeabilized by 0.5% NP40 (Sigma) and
462 incubated with 0.5% BSA (Sigma). Following primary and secondary antibodies were used;
463 CENP-C (MBL), Tubulin (Sigma), GFP (Thermo), B56-alpha (BD Biosciences), Plk1 (Santa
464 Cruz), Astrin (Sigma), Hec1/9G3 (Abcam), Hec1 pS55 (GeneTex), anti-mouse IgG Alexa 488
465 (min X, JacksonImmuno research), anti-guinea pig IgG Rhodamine Red X (min X, Jackson
466 immune research), anti-guinea pig IgG Alexa 647 (min X, JacksonImmuno research), anti-rabbit
467 IgG Alexa-488 (JacksonImmuno research) and anti-rabbit Alexa 647 (min X, Jackson immune
468 research). Stained samples were imaged both CSU W1 spinning disc confocal and CSU W1

469 SoRa super-resolution (Yokogawa) confocal microscope (Loi et al, 2023). These spinning disc
470 confocal units were equipped with a Nikon Ti2 inverted microscope with a Hamamatsu Fusion
471 camera, Shiraito PureBox (TokaiHit), and a TIRF SR 100x objective (NA = 1.49). The microscope
472 system was controlled by Nikon Elements software (Nikon). Figure 3B images were generated
473 using Imaris software (Andor).
474

475 **Image analysis**

476 Image analysis was performed using Nikon Elements software (Nikon) or Metamorph (Molecular
477 Devices). Mitotic stages and errors were determined by nuclear staining. The mitotic duration
478 was defined as the time from nuclear envelope breakdown (NEBD) to anaphase onset.
479 Timepoints of formation and loss of metaphase plate were documented. CFP signals were used
480 as a marker for infected cells. Tubulin-mNeonGreen was used for quantifying numbers of spindle
481 poles and monitoring their dynamics. Spindle pole distance was measured when spindle poles
482 were maximally stretched in high-temporal live cell images using Nikon Elements.
483

484 **Cell cycle phase analysis**

485 To track cell cycle progression, H2B signals were measured over time using Nikon NIS Elements
486 on time lapse images of Cal51 cells. Signal intensities were measured manually and the local

487 background correction method (Loi *et al.*, 2023; Suzuki *et al*, 2015) was applied to accurately
488 quantify chromatin signal intensity. Signals were collected in this manner at 18-30 min intervals.
489 The duration of each cell cycle stage was determined by analyzing changes in the H2B-mScarlet
490 signal over time.
491

492 **Polar chromosome quantification**

493 Cell segmentation and measurements of chromosome distribution were performed using the
494 Nikon NIS Elements program. First, the region-of-interest (ROI) tool was used to select
495 chromosomes located at each pole or at the equator. Corrected signal intensity was calculated
496 using a local background correction method (Suzuki *et al.*, 2015). Measurements were made for
497 every 6 minutes for the first 2 hours after NEBD, and for every ~1.5 hours subsequently. For
498 each time point, the percentage of polar chromosomes was calculated using the following
499 formula: (Corrected intensity of Pole1+Pole2)*100/(Corrected intensity of
500 Pole1+Pole2+Equator).
501

502 **Spindle rotation measurements**

503 Measurements of spindle rotation were performed using the Nikon Elements program's Manual
504 Measurement tool. Cells were observed after NEBD and the free angle tool was used to measure

505 the absolute value of the spindle rotation angle traced from using either the spindle pole or the
506 equatorial chromosomes as a reference. For control cells, measurements were made for each
507 consecutive frame from the first frame where a spindle appeared until the first frame at the onset
508 of anaphase. For Vif-expressing cells measurements were made for frames whenever a visually
509 significant angle was traced. Data was exported to Excel. The Matplotlib library in Python was
510 used to make polar plots, with time plotted as radius and angle traced plotted as theta.
511

512 **Statistics**

513 All experiments were independently repeated 2-3 times for mitotic duration measurements. p-
514 values were calculated using one-way ANOVA and the two-tailed Student's t-test. p-values <
515 0.05 were considered significant. In the figures, p-values are denoted as * for ≤0.05, ** for ≤0.01,
516 *** for ≤0.001 and **** for ≤0.0001.
517

518 **Transduction and infection**

519 For infections, growth media was replaced with viral supernatants carrying VSV-G-pseudo typed
520 HIV-1 CFP reporter viruses (Vif-positive or Vif-negative) at a multiplicity of infection of ~1, with
521 the viruses engineered and produced as previously described (Evans et al., 2018).
522

523 ## References

524 Anna AY, Deretic J, Hoel CM, Hinman AW, Cimini D, Welburn JP, Maresca TJ (2015) Aurora A kinase contributes to a pole-based
525 error correction pathway. *Current Biology* 25: 1842-1851
526 Augustine T, Chaudhary P, Gupta K, Islam S, Ghosh P, Santra MK, Mitra D (2017) Cyclin F/FBXO1 Interacts with HIV-1 Viral
527 Infectivity Factor (Vif) and Restricts Progeny Virion Infectivity by Ubiquitination and Proteasomal Degradation of Vif Protein
528 through SCFcyclin F E3 Ligase Machinery. *Journal of Biological Chemistry* 292: 5349-5363
529 Barr AR, Gergely F (2007) Aurora-A: the maker and breaker of spindle poles. *Journal of Cell Science* 120: 2987-2996
530 Bartz SR, Rogel ME, Emerman M (1996) Human immunodeficiency virus type 1 cell cycle control: Vpr is cytostatic and mediates
531 G2 accumulation by a mechanism which differs from DNA damage checkpoint control. *J Virol* 70: 2324-2331
532 Cheeseman IM, Chappie JS, Wilson-Kubalek EM, Desai A (2006) The conserved KMN network constitutes the core
533 microtubule-binding site of the kinetochore. *Cell* 127: 983-997
534 Chiu Y-L, Greene WC (2009) APOBEC3G: an intracellular centurion. *Philosophical Transactions of the Royal Society B: Biological*
535 *Sciences* 364: 689-703
536 Chmátal L, Yang K, Schultz RM, Lampson MA (2015) Spatial regulation of kinetochore microtubule attachments by
537 destabilization at spindle poles in meiosis I. *Current Biology* 25: 1835-1841
538 Choi HJ, Fukui M, Zhu BT (2011) Role of Cyclin B1/Cdc2 Up-Regulation in the Development of Mitotic Prometaphase Arrest in
539 Human Breast Cancer Cells Treated with Nocodazole. *Plos One* 6
540 Clijsters L, Hoencamp C, Calis JJA, Marzio A, Handgraaf SM, Cuitino MC, Rosenberg BR, Leone G, Pagano M (2019) Cyclin F
541 Controls Cell-Cycle Transcriptional Outputs by Directing the Degradation of the Three Activator E2Fs. *Molecular Cell* 74: 1264-
542 1277.e1267
543 Cohen MS, Chen YQ, McCauley M, Gamble T, Hosseinipour MC, Kumarasamy N, Hakim JG, Kumwenda J, Grinsztejn B, Pilotto
544 JHS *et al* (2016) Antiretroviral Therapy for the Prevention of HIV-1 Transmission. *New England Journal of Medicine* 375: 830-
545 839
546 Colicino EG, Hehnly H (2018) Regulating a key mitotic regulator, polo-like kinase 1 (PLK1). *Cytoskeleton (Hoboken)* 75: 481-494
547 Conti D, Gul P, Islam A, Martín-Durán JM, Pickersgill RW, Draviam VM (2019) Kinetochores attached to microtubule-ends are
548 stabilised by Astrin bound PP1 to ensure proper chromosome segregation. *eLife* 8: e49325
549 Conticello SG, Harris RS, Neuberger MS (2003) The Vif protein of HIV triggers degradation of the human antiretroviral DNA
550 deaminase APOBEC3G. *Current Biology* 13: 2009-2013
551 Das AT, Tenenbaum L, Berkhout B (2016) Tet-On Systems For Doxycycline-inducible Gene Expression. *Curr Gene Ther* 16: 156-
552 167
553 Deeks SG, Overbaugh J, Phillips A, Buchbinder S (2015) HIV infection. *Nature Reviews Disease Primers* 1
554 DeHart JL, Bosque A, Harris RS, Planelles V (2008) Human immunodeficiency virus type 1 Vif induces cell cycle delay via
555 recruitment of the same E3 ubiquitin ligase complex that targets APOBEC3 proteins for degradation. *Journal of virology* 82:
556 9265-9272
557 DeLuca JG, 2017. Aurora A kinase function at kinetochores, Cold Spring Harbor Symposia on Quantitative Biology. Cold Spring

558 Harbor Laboratory Press, pp. 91-99.
559 DeLuca KF, Lens SMA, DeLuca JG (2011) Temporal changes in Hec1 phosphorylation control kinetochore–microtubule
560 attachment stability during mitosis. *Journal of Cell Science* 124: 622-634
561 Doitsh G, Greene WC (2016) Dissecting How CD4 T Cells Are Lost During HIV Infection. *Cell Host Microbe* 19: 280-291
562 Du J, Rui Y, Zheng W, Li P, Kang J, Zhao K, Sun T, Yu X-F (2019) Vif-CBFβ interaction is essential for Vif-induced cell cycle arrest.
563 *Biochemical and biophysical research communications* 511: 910-915
564 Dunsch AK, Linnane E, Barr FA, Gruneberg U (2011) The astrin–kinastrin/SKAP complex localizes to microtubule plus ends and
565 facilitates chromosome alignment. *Journal of Cell Biology* 192: 959-968
566 Elder RT (2002) HIV-1 VPR modulates cell cycle G2/M transition through an alternative cellular mechanism other than the
567 classic mitotic checkpoints. *Frontiers in Bioscience* 7
568 Emerman M (1996) HIV-1, Vpr and the cell cycle. *Current Biology* 6: 1096-1103
569 Enrico TP, Stallaert W, Wick ET, Ngoi P, Wang X, Rubin SM, Brown NG, Purvis JE, Emanuele MJ (2021) Cyclin F drives proliferation
570 through SCF-dependent degradation of the retinoblastoma-like tumor suppressor p130/RBL2. *eLife* 10
571 Evans EL, Becker JT, Fricke SL, Patel K, Sherer NM, Kirchhoff F (2018) HIV-1 Vif's Capacity To Manipulate the Cell Cycle Is Species
572 Specific. *Journal of Virology* 92
573 Foley EA, Kapoor TM (2013) Microtubule attachment and spindle assembly checkpoint signalling at the kinetochore. *Nat Rev*
574 *Mol Cell Bio* 14: 25-37
575 Foley EA, Maldonado M, Kapoor TM (2011) Formation of stable attachments between kinetochores and microtubules
576 depends on the B56-PP2A phosphatase. *Nat Cell Biol* 13: 1265-U1216
577 Friese A, Faesen AC, Huis in 't Veld PJ, Fischböck J, Prumbaum D, Petrovic A, Raunser S, Herzog F, Musacchio A (2016) Molecular
578 requirements for the inter-subunit interaction and kinetochore recruitment of SKAP and Astrin. *Nature Communications* 7:
579 11407
580 Gabuzda DH, Lawrence K, Langhoff E, Terwilliger E, Dorfman T, Haseltine WA, Sodroski J (1992) Role of Vif in Replication of
581 Human-Immunodeficiency-Virus Type-1 in Cd4+ T Lymphocytes. *Journal of Virology* 66: 6489-6495
582 Greenwood EJD, Matheson NJ, Wals K, van den Boomen DJH, Antrobus R, Williamson JC, Lehner PJ (2016) Temporal proteomic
583 analysis of HIV infection reveals remodelling of the host phosphoproteome by lentiviral Vif variants. *Elife* 5: e18296
584 Grulich AE, van Leeuwen MT, Falster MO, Vajdic CM (2007) Incidence of cancers in people with HIV/AIDS compared with
585 immunosuppressed transplant recipients: a meta-analysis. *The Lancet* 370: 59-67
586 Hall R, Ahern LM, Yap MW, Tsai M-HC, Boucherit VC, Takaki T, Boulton SJ, Bishop KN (2024) HIV-1 Vpr causes separate cell cycle
587 arrests in G2 and M that activate alternative DNA damage pathways. *bioRxiv*: 2024.2004. 2002.587683
588 He J, Choe S, Walker R, Di Marzio P, Morgan DO, Landau NR (1995) Human immunodeficiency virus type 1 viral protein R (Vpr)
589 arrests cells in the G2 phase of the cell cycle by inhibiting p34cdc2 activity. *J Virol* 69: 6705-6711
590 Hernández-Ramírez RU, Shiels MS, Dubrow R, Engels EA (2017) Cancer risk in HIV-infected people in the USA from 1996 to
591 2012: a population-based, registry-linkage study. *The Lancet HIV* 4: e495-e504
592 Izumi T, Io K, Matsui M, Shirakawa K, Shinohara M, Nagai Y, Kawahara M, Kobayashi M, Kondoh H, Misawa N *et al* (2010) HIV-
593 1 viral infectivity factor interacts with TP53 to induce G2 cell cycle arrest and positively regulate viral replication. *Proceedings*

594 *of the National Academy of Sciences* 107: 20798-20803
595 Jouvenet N, Simon SM, Bieniasz PD (2009) Imaging the interaction of HIV-1 genomes and Gag during assembly of individual
596 viral particles. *Proceedings of the National Academy of Sciences* 106: 19114-19119
597 Jowett JB, Planelles V, Poon B, Shah NP, Chen ML, Chen IS (1995) The human immunodeficiency virus type 1 vpr gene arrests
598 infected T cells in the G2 + M phase of the cell cycle. *J Virol* 69: 6304-6313
599 Kettenbach AN, Schweppe DK, Faherty BK, Pechenick D, Pletnev AA, Gerber SA (2011) Quantitative Phosphoproteomics
600 Identifies Substrates and Functional Modules of Aurora and Polo-Like Kinase Activities in Mitotic Cells. *Science Signaling* 4:
601 rs5-rs5
602 Lee SJ, Rodriguez-Bravo V, Kim H, Datta S, Foley EA (2017) The PP2AB56 phosphatase promotes the association of Cdc20 with
603 APC/C in mitosis. *Journal of cell science*
604 Loi J, Qu X, Suzuki A (2023) Semi-automated 3D fluorescence speckle analyzer (3D-Speckler) for microscope calibration and
605 nanoscale measurement. *The Journal of cell biology* 222
606 Lynch AR, Arp NL, Zhou AS, Weaver BA, Burkard ME (2022) Quantifying chromosomal instability from intratumoral karyotype
607 diversity using agent-based modeling and Bayesian inference. *Elife* 11: e69799
608 Malim MH, Emerman M (2008) HIV-1 accessory proteins—ensuring viral survival in a hostile environment. *Cell host & microbe*
609 3: 388-398
610 Manning AL, Bakhoum SF, Maffini S, Correia‐Melo C, Maiato H, Compton DA (2010) CLASP1, astrin and Kif2b form a
611 molecular switch that regulates kinetochore‐microtubule dynamics to promote mitotic progression and fidelity. *The EMBO*
612 *Journal* 29: 3531-3543-3543
613 Mardin BR, Drainas AP, Waszak SM, Weischenfeldt J, Isokane M, Stütz AM, Raeder B, Efthymiopoulos T, Buccitelli C, Segura-
614 Wang M *et al* (2015) A cell-based model system links chromothripsis with hyperploidy. *Mol Syst Biol* 11
615 Marelli S, Williamson JC, Protasio AV, Naamati A, Greenwood EJD, Deane JE, Lehner PJ, Matheson NJ (2020) Antagonism of
616 PP2A is an independent and conserved function of HIV-1 Vif and causes cell cycle arrest. *eLife* 9
617 Marin M, Rose KM, Kozak SL, Kabat D (2003) HIV-1 Vif protein binds the editing enzyme APOBEC3G and induces its degradation.
618 *Nature Medicine* 9: 1398-1403
619 McVey SL, Cosby JK, Nannas NJ (2021) Aurora B Tension Sensing Mechanisms in the Kinetochore Ensure Accurate Chromosome
620 Segregation. *Int J Mol Sci* 22
621 Mustafa F, Robinson HL (1993) Context-dependent role of human immunodeficiency virus type 1 auxiliary genes in the
622 establishment of chronic virus producers. *J Virol* 67: 6909-6915
623 Muthumani K, Choo AY, Premkumar A, Hwang DS, Thieu KP, Desai BM, Weiner DB (2005) Human immunodeficiency virus type
624 1 (HIV-1) Vpr-regulated cell death: insights into mechanism. *Cell Death Differ* 12: 962-970
625 Nagata K, Shindo K, Matsui Y, Shirakawa K, Takaori-Kondo A (2020) Critical role of PP2A-B56 family protein degradation in HIV-
626 1 Vif mediated G2 cell cycle arrest. *Biochemical and biophysical research communications* 527: 257-263
627 Nardacci R, Perfettini JL, Grieco L, Thieffry D, Kroemer G, Piacentini M (2015) Syncytial apoptosis signaling network induced
628 by the HIV-1 envelope glycoprotein complex: an overview. *Cell Death Dis* 6
629 Nguyen DH, Hildreth JEK (2000) Evidence for Budding of Human Immunodeficiency Virus Type 1 Selectively from Glycolipid-

630 Enriched Membrane Lipid Rafts. *Journal of Virology* 74: 3264-3272
631 Okada A, Iwatani Y (2016) APOBEC3G-Mediated G-to-A Hypermutation of the HIV-1 Genome: The Missing Link in Antiviral
632 Molecular Mechanisms. *Frontiers in Microbiology* 7
633 Olivier M, Eeles R, Hollstein M, Khan MA, Harris CC, Hainaut P (2002) The IARC TP53 database: New online mutation analysis
634 and recommendations to users. *Human Mutation* 19: 607-614
635 Ono A, Freed EO (2001) Plasma membrane rafts play a critical role in HIV-1 assembly and release. *Proceedings of the National*
636 *Academy of Sciences* 98: 13925-13930
637 Parkin DM (2006) The global health burden of infection-associated cancers in the year 2002. *Int J Cancer* 118: 3030-3044
638 Poser E, Caous R, Gruneberg U, Barr FA (2019) Aurora A promotes chromosome congression by activating the condensin-
639 dependent pool of KIF4A. *Journal of Cell Biology* 219
640 Sakai K, Barnitz RA, Chaigne-Delalande B, Bidère N, Lenardo MJ (2011) Human Immunodeficiency Virus Type 1 Vif causes
641 dysfunction of Cdk1 and CyclinB1: implications for cell cycle arrest. *Virology Journal* 8
642 Sakai K, Dimas J, Lenardo MJ (2006) The Vif and Vpr accessory proteins independently cause HIV-1-induced T cell cytopathicity
643 and cell cycle arrest. *Proceedings of the National Academy of Sciences* 103: 3369-3374
644 Salamango DJ, Ikeda T, Moghadasi SA, Wang J, McCann JL, Serebrenik AA, Ebrahimi D, Jarvis MC, Brown WL, Harris RS (2019)
645 HIV-1 Vif Triggers Cell Cycle Arrest by Degrading Cellular PPP2R5 Phospho-regulators. *Cell Reports* 29: 1057-1065.e1054
646 Salamango DJ, McCann JL, Demir Ö, Becker JT, Wang J, Lingappa JR, Temiz NA, Brown WL, Amaro RE, Harris RS *et al* (2020)
647 Functional and Structural Insights into a Vif/PPP2R5 Complex Elucidated Using Patient HIV-1 Isolates and Computational
648 Modeling. *Journal of Virology* 94
649 Saurin AT (2018) Kinase and Phosphatase Cross-Talk at the Kinetochore. *Front Cell Dev Biol* 6: 62
650 Schmidt JC, Kiyomitsu T, Hori T, Backer CB, Fukagawa T, Cheeseman IM (2010) Aurora B kinase controls the targeting of the
651 Astrin–SKAP complex to bioriented kinetochores. *Journal of Cell Biology* 191: 269-280
652 Schuhmacher D, Sontag J-M, Sontag E (2019) Protein Phosphatase 2A: More Than a Passenger in the Regulation of Epithelial
653 Cell–Cell Junctions. *Frontiers in Cell and Developmental Biology* 7
654 Scribano CM, Wan J, Esbona K, Tucker JB, Lasek A, Zhou AS, Zasadil LM, Molini R, Fitzgerald J, Lager AM *et al* (2021)
655 Chromosomal instability sensitizes patient breast tumors to multipolar divisions induced by paclitaxel. *Science Translational*
656 *Medicine* 13
657 Sheehy AM, Gaddis NC, Malim MH (2003) The antiretroviral enzyme APOBEC3G is degraded by the proteasome in response
658 to HIV-1 Vif. *Nature Medicine* 9: 1404-1407
659 Sivakumar S, Gorbsky GJ (2017) Phosphatase-regulated recruitment of the spindle- and kinetochore-associated (Ska) complex
660 to kinetochores. *Biol Open* 6: 1672-1679
661 Smith RJ, Cordeiro MH, Davey NE, Vallardi G, Ciliberto A, Gross F, Saurin AT (2019) PP1 and PP2A Use Opposite Phospho-
662 dependencies to Control Distinct Processes at the Kinetochore. *Cell Rep* 28: 2206-2219 e2208
663 St Clair S, Giono L, Varmeh-Ziaie S, Resnick-Silverman L, Liu WJ, Padi A, Dastidar J, DaCosta A, Mattia M, Manfredi JJ (2004)
664 DNA damage-induced downregulation of Cdc25C is mediated by p53 via two independent mechanisms:: One involves direct
665 binding to the

666 promoter. *Molecular Cell* 16: 725-736
667 Stark GR, Taylor WR (2006) Control of the G2/M transition. *Molecular Biotechnology* 32: 227-248
668 Stopak K, de Noronha C, Yonemoto W, Greene WC (2003) HIV-1 Vif blocks the antiviral activity of APOBEC3G by impairing both
669 its translation and intracellular stability. *Molecular cell* 12: 591-601
670 Suzuki A, Badger BL, Salmon ED (2015) A quantitative description of Ndc80 complex linkage to human kinetochores. *Nature*
671 *communications* 6: 8161
672 Swanstrom R, Coffin J (2012) HIV-1 Pathogenesis: The Virus. *Cold Spring Harbor Perspectives in Medicine* 2: a007443-a007443
673 Taylor WR, Stark GR (2001) Regulation of the G2/M transition by p53. *Oncogene* 20: 1803-1815
674 Vallardi G, Cordeiro MH, Saurin AT (2017) A Kinase-Phosphatase Network that Regulates Kinetochore-Microtubule
675 Attachments and the SAC. *Prog Mol Subcell Biol* 56: 457-484
676 Vidya Vijayan KK, Karthigeyan KP, Tripathi SP, Hanna LE (2017) Pathophysiology of CD4+ T-Cell Depletion in HIV-1 and HIV-2
677 Infections. *Front Immunol* 8: 580
678 Wandke C, Barisic M, Sigl R, Rauch V, Wolf F, Amaro AC, Tan CH, Pereira AJ, Kutay U, Maiato H *et al* (2012) Human
679 chromokinesins promote chromosome congression and spindle microtubule dynamics during mitosis. *Journal of Cell Biology*
680 198: 847-863
681 Wang J, Reuschel EL, Shackelford JM, Jeang L, Shivers DK, Diehl JA, Yu X-F, Finkel TH (2011) HIV-1 Vif promotes the G1- to S-
682 phase cell-cycle transition. *Blood* 117: 1260-1269
683 Wang J, Shackelford JM, Selliah N, Shivers DK, O'Neill E, Garcia JV, Muthumani K, Weiner D, Yu X-F, Gabuzda D *et al* (2008) The
684 HIV-1 Vif Protein Mediates Degradation of Vpr and Reduces Vpr-Induced Cell Cycle Arrest. *DNA and Cell Biology* 27: 267-277
685 Yu X, Yu Y, Liu B, Luo K, Kong W, Mao P, Yu X-F (2003) Induction of APOBEC3G Ubiquitination and Degradation by an HIV-1 Vif-
686 Cul5-SCF Complex. *Science* 302: 1056-1060
687 Zhang P, Zhang Y, Gao K, Wang Y, Jin X, Wei Y, Saiyin H, Wang D, Peng J, Ma J *et al* (2015) ASPP1/2-PP1 complexes are required
688 for chromosome segregation and kinetochore-microtubule attachments. *Oncotarget* 6: 41550-41565
689 Zhao K, Du J, Rui Y, Zheng W, Kang J, Hou J, Wang K, Zhang W, Simon VA, Yu X-F (2015) Evolutionarily conserved pressure for
690 the existence of distinct G2/M cell cycle arrest and A3H inactivation functions in HIV-1 Vif. *Cell cycle* 14: 838-847

691

692

693 **Figure Legends**

694 **Figure 1: Vif and Vpr induce distinct forms of mitotic arrest.**

695 (A) Representative live cell image for Cal51 cells with H2B-mScarlet and Tubulin-mNeonGreen
696 expressing Control, Vif, Vpr, or Vif+Vpr reporter viruses. (B) Average mitotic duration of Cal51
697 cells expressing respective reporter virus (n=100 for each from two replicates). (C) Frequency
698 of cell fate after mitosis for Cal51 cells expressing respective reporter virus. (n=100 for each
699 from two replicates)

700

701 **Figure 2: Vif induces robust pseudo-metaphase arrest.**

702 (A) Representative live cell images for Cal51 cells with H2B-mScarlet and Tubulin-mNeonGreen
703 expressing Control reporter virus. (B) Representative live cell image for Cal51 cells expressing
704 Vif reporter virus. (C) Frequency of cells that achieve metaphase plate and time taken to achieve
705 metaphase plate for cells in (A) and (B) (n=100 for each from two replicates). (D) Representative
706 live-cell images of Vif conditional expressed HeLa cell with or without Doxycycline. (E) Average
707 mitotic duration in condition (D) (n=100 cells for each from two replicates). (F) Quantification of
708 viable cells over time after Dox induction. (G) Quantification of apoptotic cells after Dox induction.

709

710 **Figure 3: Vif does not alter G1 or S phase progression, accelerates G2 progression, and**

711 **induces pseudo-metaphase arrest independent of p53**

712 (A) Top: Representative image of Cal51 cells progressing through G1, S, and G2. Bottom:
713 Representative trace for relative signal intensity of the nucleus through cell cycle. (B) Average
714 duration of G1, S, and G2 phases in Control and Vif-expressing cells (n= 9 for Control and 11
715 for Vif, from two replicates). (C) Total cell cycle duration for Control and Vif-expressing cells. (D)
716 Representative live cell images for Control and Vif-expressing WT or p35KO RPE1 cells. (E)
717 Average mitotic duration in WT or p53KO RPE1 cells (n= >85 cells, from two replicates). (F)
718 Frequency of cells which achieve metaphase plate for cells in (E). (G) Average time taken to
719 achieve metaphase plate for cells in (F).

720

721 **Figure 4: Vif induces polar chromosomes, multi-polar spindles, and abnormal**
722 **chromosome movements**

723 (A) Representative immunofluorescence images labeled for CENP-C (as a kinetochore marker),
724 microtubule, and DNA in Control and Vif-expressing HeLa cells. (B) Example super-resolution
725 images labeled for CENP-C, microtubule, and DNA in Vif-expressed HeLa cells showing polar
726 chromosomes. (C) Representative live cell image of Vif-expressing cells where polar
727 chromosomes were quantified by compartmentalizing polar regions. Bottom: Quantification of
728 polar chromosome frequency overtime. (D) Representative high-temporal live cell images (6

729 minutes interval) showing rapid chromosome moving towards and away from the spindle poles.
730 (E) Fraction of Cal51 cells showing abnormal number of poles at some point during mitosis. (F)
731 Top: Representative images of maximum mitotic spindle length for Control and Vif-expressing
732 Cal51 cells. Bottom: Average maximum mitotic spindle length of Control and Vif-expressing cells.
733 (G) Top: Representative live cell image of Control and Vif-expressing Cal51 cells over time
734 showing dynamic spindle spinning. Center: Representative figures showing relative orientation
735 (angle) of the spindle axis over time (radius). Bottom: Average total angle swept during mitosis.
736

737 **Figure 5: Vif, but not Vpr, disrupts the proper localization of PP2A-B56 at the kinetochores**
738 (A) Representative maximum intensity projection of fixed Control and Vif-expressing HeLa cells
739 with or without nocodazole treatment, immunofluorescently labeled for B56, CENP-C, and DNA.
740 (B) Representative maximum intensity projection of fixed Control and Vpr-expressing HeLa cells,
741 immunofluorescently labeled for B56, CENP-C, and DNA. (C) Average B56 level at kinetochores
742 for cells in (A) and (B) (n=200 kinetochores over 8 cells from two independent replicates for
743 each). (D) Representative fixed-cell immunofluorescent image of HeLa cells expressing Vif,
744 immunofluorescently labeled for Plk1, CENP-C, and DNA. (E) Average Plk1 level at kinetochores
745 for cells in (D) (n=200 kinetochores over 8 cells from two independent replicates for each).
746

747 **Figure 6: Vif impairs stable and balanced kinetochore microtubule attachments**

748 (A) Left: Representative maximum intensity projection of fixed Control and Vif-expressing HeLa
749 cells immunofluorescently labeled for CENP-C, Astrin, and DNA along with representative sister
750 kinetochore pairs, Right: Illustrative interpretation of images on the left. (B) Average Astrin and
751 CENP-C level at kinetochores for cells in (A) (n = 200 kinetochores from 8 cells from two
752 independent replicates for each) (C) Comparison of Astrin and CENP-C on sister kinetochores,
753 values normalized with formula: 1 – (lower intensity value/higher intensity value). (D)
754 Representative image of fixed Control and Vif-expressing HeLa cells immunofluorescently
755 labeled for CENP-C, pHec1(S55), and DNA along with representative sister kinetochore pairs.
756 (E) Average pHec1(S55) level at kinetochores for cells in (D). (n = 200 kinetochores from 8 cells
757 from two independent replicates for each). (F) Comparison of pHec1(S55) on sister kinetochores,
758 values normalized with formula: 1 – (lower intensity value/higher intensity value). (G)
759 Representative fixed-cell immunofluorescent image of HeLa cells expressing Vif,
760 immunofluorescently labeled for Hec1, CENP-C, and DNA. (H) Average Hec1 level at
761 kinetochores for cells in (G) (n=200 kinetochores over 8 cells from two independent replicates
762 for each).

763

764 **Figure 7: Proposed model for the molecular mechanism underlying Vif's pseudo-**

765 **metaphase arrest**

766 Top: Cartoon model depicting metaphase alignment of Control cells followed by anaphase.
767 Middle: Cartoon model depicting pseudo-metaphase alignment of Vif-expressing cells with
768 unbalanced microtubule attachment followed by three-step polar chromosome cycle. Bottom:
769 Cartoon depiction of three-step polar chromosome cycle, (1) chromosome at the equator is
770 pulled towards pole due to unbalanced pulling force, (2) kinetochore-microtubule destabilization
771 at the spindle pole, (3) equator-directed movement of chromosome for realignment.

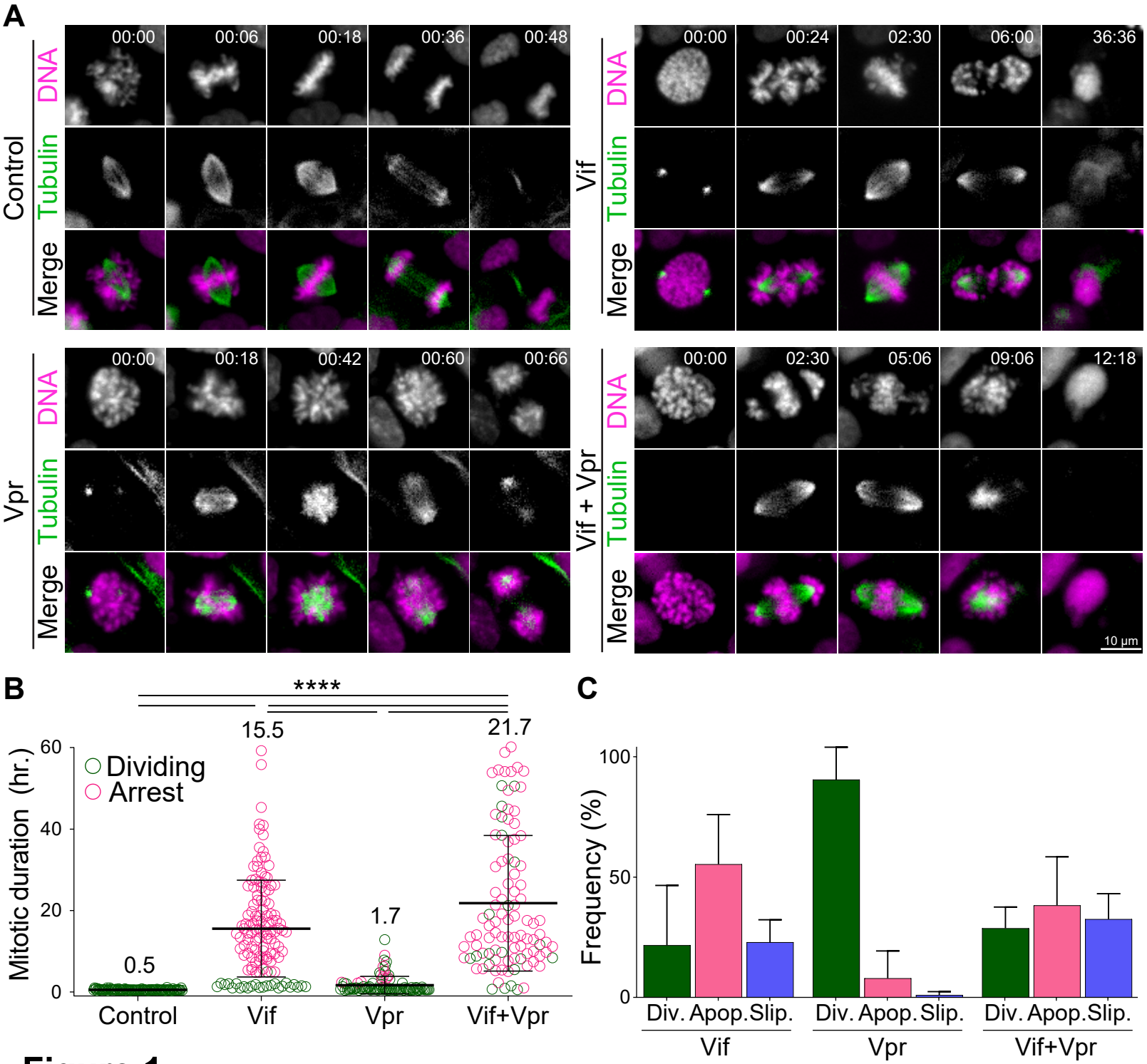
A
Control
Vif
Vpr
Vif + Vpr
DNA
Tubulin
Merge
00:00
00:06
00:18
00:36
00:48
00:24
02:30
06:00
36:36
00:42
00:60
00:66
05:06
09:06
12:18
10 µm
B
****
Mitotic duration (hr.)
Dividing
Arrest
0.5
15.5
1.7
21.7
Control
Vif
Vpr
Vif+Vpr
C
Frequency (%)
Div.
Apop.
Slip.
Vif
Vpr
Vif+Vpr

Figure 1

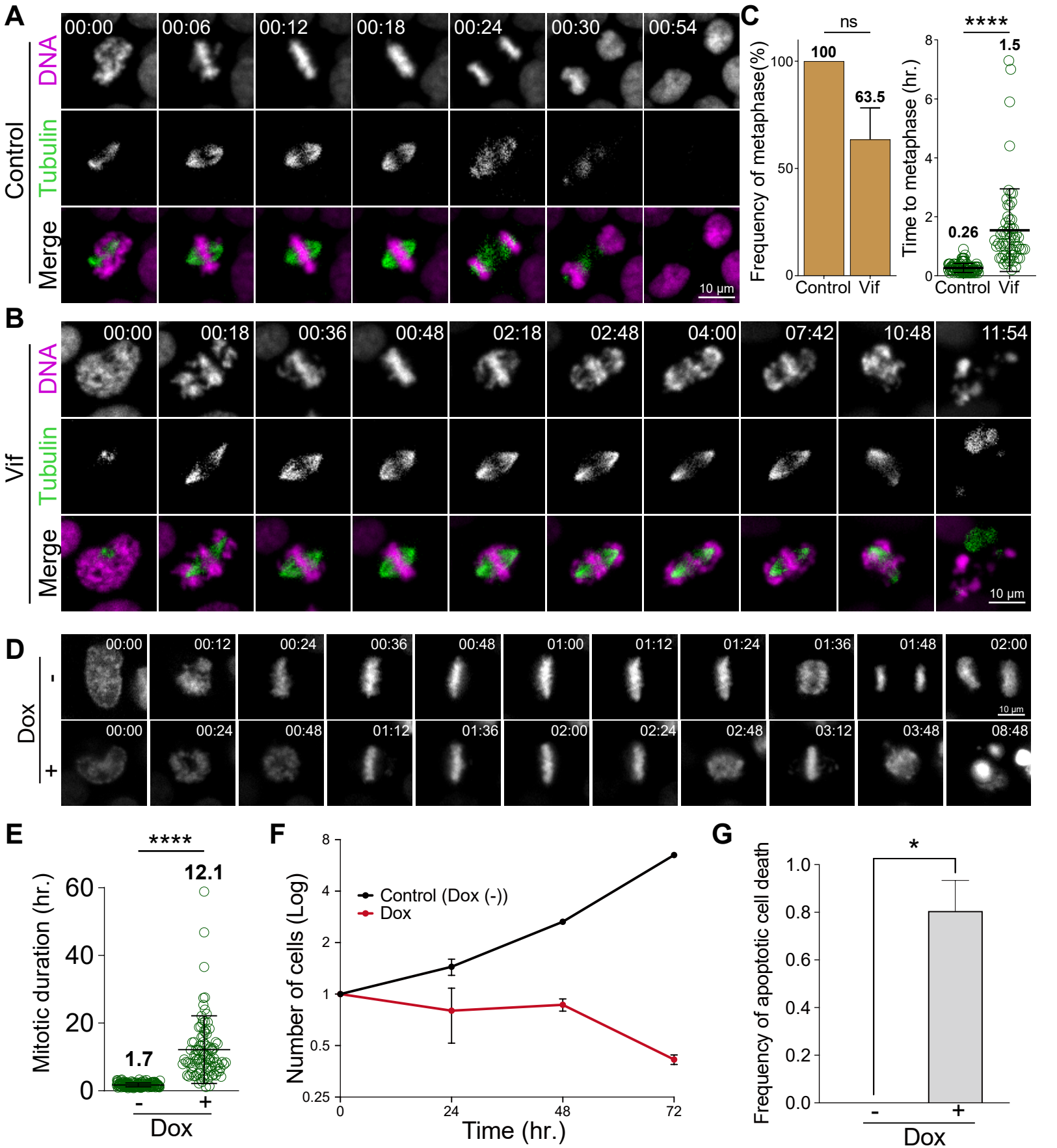
A
Control
DNA
Tubulin
Merge
00:00
00:06
00:12
00:18
00:24
00:30
00:54
10 µm
B
Vif
00:00
00:18
00:36
00:48
02:18
02:48
04:00
07:42
10:48
11:54
C
ns
****
Frequency of metaphase(%)
100
63.5
Control
Vif
Time to metaphase (hr.)
0.26
1.5
D
Dox
-
+
00:00
00:12
00:24
00:36
00:48
01:00
01:12
01:24
01:36
01:48
02:00
00:24
00:48
01:12
01:36
02:00
02:24
02:48
03:12
03:48
08:48
E
Mitotic duration (hr.)
12.1
1.7
Dox
F
Number of cells (Log)
Control (Dox (-))
Dox
Time (hr.)
G
Frequency of apoptotic cell death
*
Dox

Figure 2

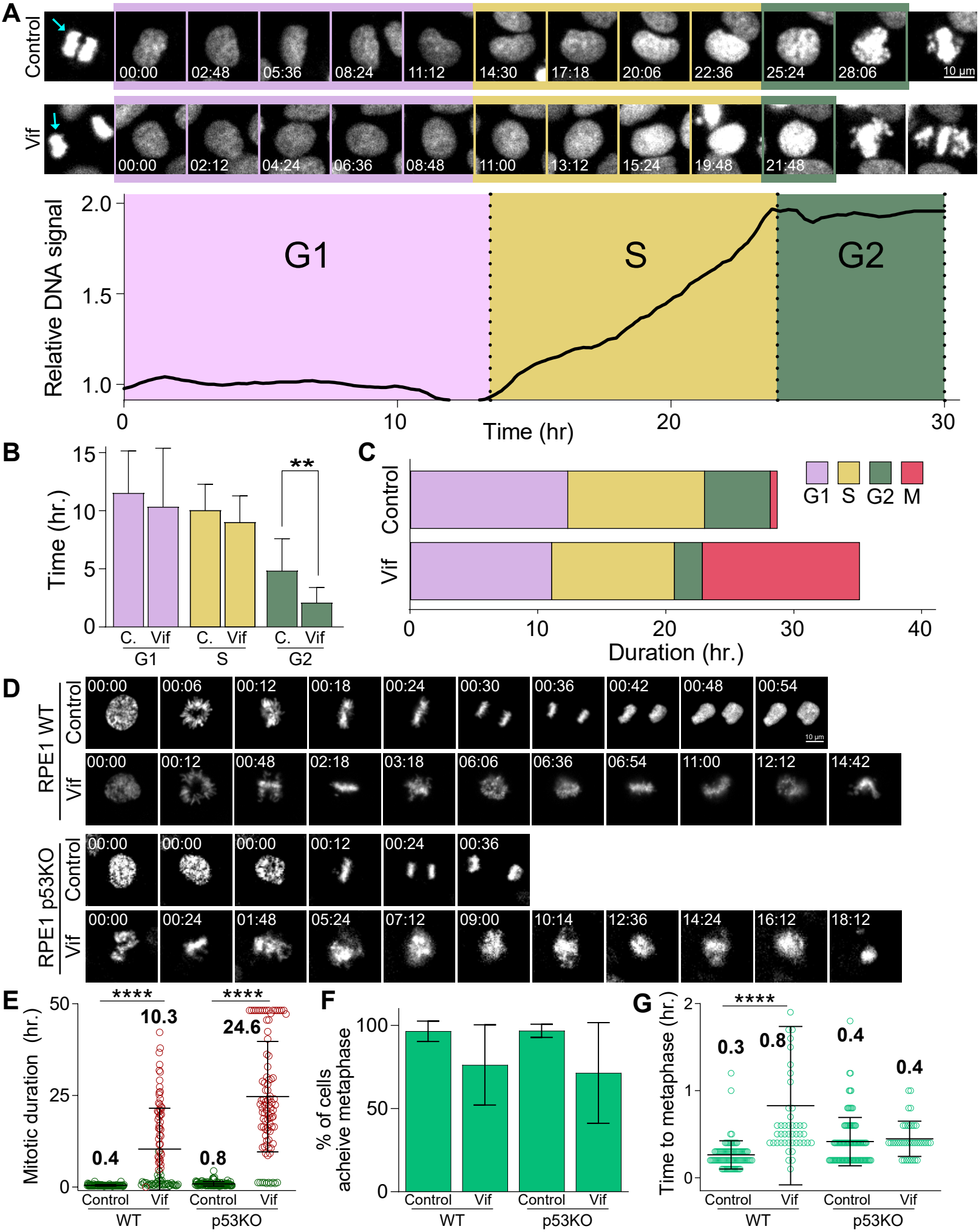
A
Control
00:00
02:48
05:36
08:24
11:12
14:30
17:18
20:06
22:36
25:24
28:06
10 µm
Vif
00:00
02:12
04:24
06:36
08:48
11:00
13:12
15:24
19:48
21:48
Relative DNA signal
2.0
1.5
1.0
G1
S
G2
0
10
20
30
Time (hr)
B
Time (hr.)
15
10
5
0
**
C. Vif
G1
S
G2
C
Control
Vif
G1 S G2 M
0
10
20
30
40
Duration (hr.)
D
RPE1 WT
Control
00:00
00:06
00:12
00:18
00:24
00:30
00:36
00:42
00:48
00:54
10 µm
Vif
00:00
00:12
00:48
02:18
03:18
06:06
06:36
06:54
11:00
12:12
14:42
RPE1 p53KO
Control
00:00
00:00
00:00
00:12
00:24
00:36
Vif
00:00
00:24
01:48
05:24
07:12
09:00
10:14
12:36
14:24
16:12
18:12
E
Mitotic duration (hr.)
50
25
0
****
10.3
0.4
****
24.6
0.8
Control
Vif
WT
p53KO
F
% of cells acheive metaphase
100
50
0
Control
Vif
WT
p53KO
G
Time to metaphase (hr.)
2
1
0
****
0.3
0.8
0.4
0.4
Control
Vif
WT
p53KO

Figure 3

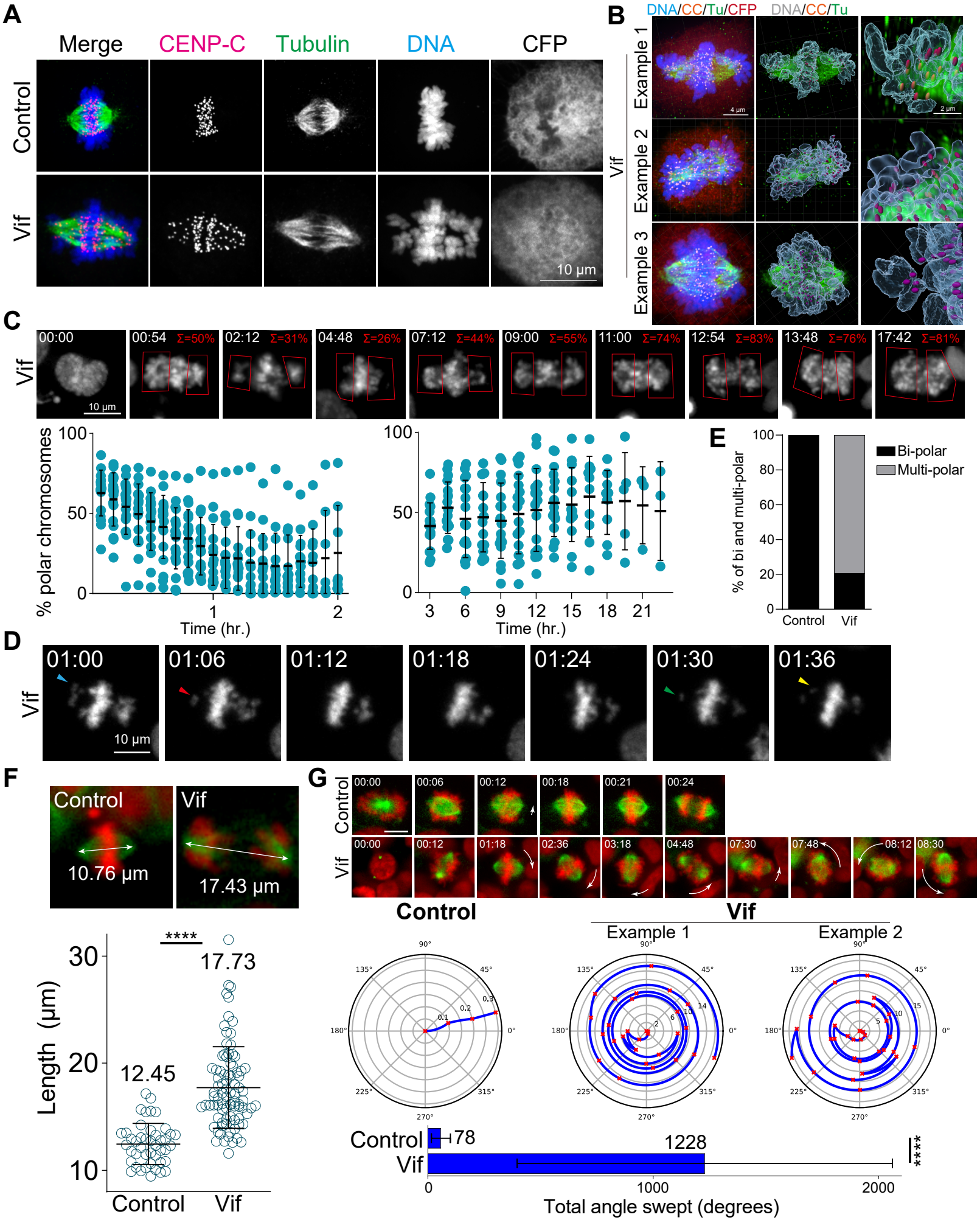
A
Merge
CENP-C
Tubulin
DNA
CFP
Control
Vif
10 µm
B
DNA/CC/Tu/CFP
DNA/CC/Tu
Example 1
Example 2
Example 3
Vif
4 µm
2 µm
C
Vif
00:00
00:54 Σ=50%
02:12 Σ=31%
04:48 Σ=26%
07:12 Σ=44%
09:00 Σ=55%
11:00 Σ=74%
12:54 Σ=83%
13:48 Σ=76%
17:42 Σ=81%
10 µm
% polar chromosomes
Time (hr.)
E
% of bi and multi-polar
Bi-polar
Multi-polar
Control
Vif
D
Vif
01:00
01:06
01:12
01:18
01:24
01:30
01:36
10 µm
F
Control
Vif
10.76 µm
17.43 µm
Length (µm)
****
12.45
17.73
Control
Vif
G
Control
Vif
00:00
00:06
00:12
00:18
00:21
00:24
00:12
01:18
02:36
03:18
04:48
07:30
07:48
08:12
08:30
Control
Vif
Example 1
Example 2
Control
Vif
78
1228
****
Total angle swept (degrees)

Figure 4

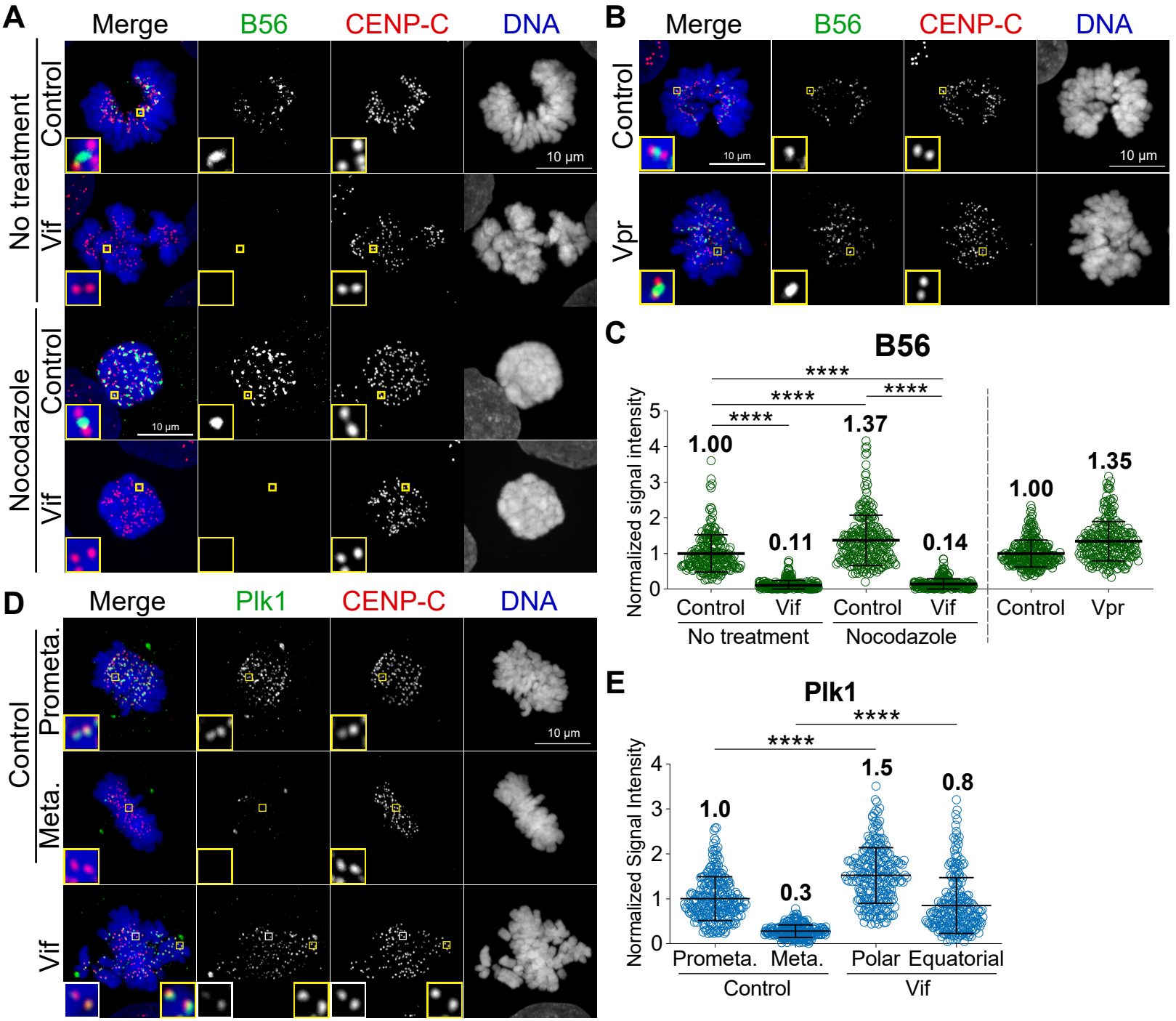
A
Merge
B56
CENP-C
DNA
No treatment
Control
Vif
Nocodazole
Control
Vif
10 µm
B
Merge
B56
CENP-C
DNA
Control
Vpr
10 µm
C
B56
Normalized signal intensity
****
****
****
****
1.00
0.11
1.37
0.14
1.00
1.35
Control
Vif
Control
Vif
Control
Vpr
No treatment
Nocodazole
D
Merge
Plk1
CENP-C
DNA
Control
Prometa.
Meta.
Vif
10 µm
E
Plk1
Normalized Signal Intensity
****
****
1.0
0.3
1.5
0.8
Prometa.
Meta.
Polar
Equatorial
Control
Vif

Figure 5

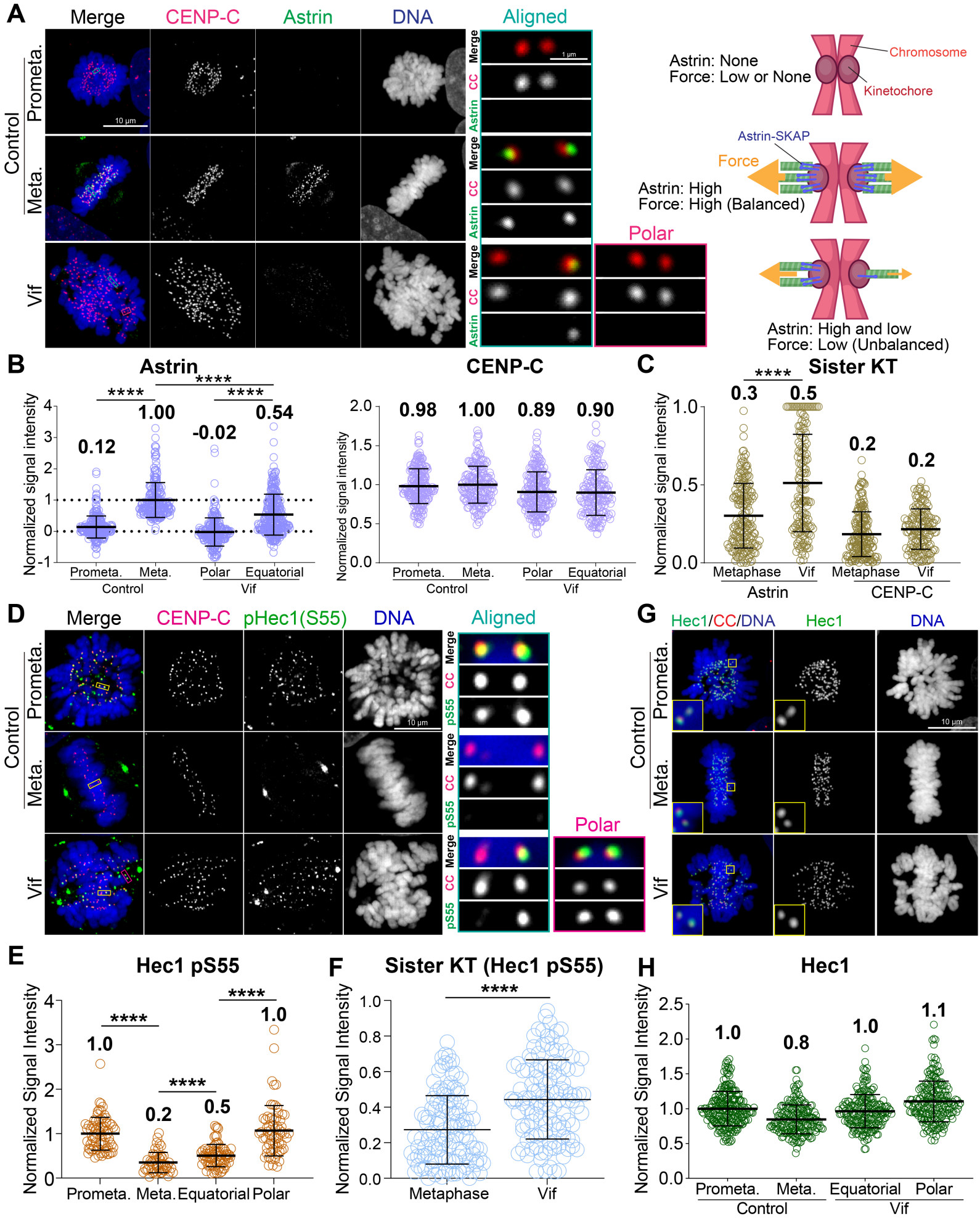
A
Merge
CENP-C
Astrin
DNA
Aligned
Control
Prometa.
Meta.
Vif
10 µm
1 µm
Merge
CC
Astrin
Polar
Astrin: None
Force: Low or None
Chromosome
Kinetochore
Astrin-SKAP
Force
Astrin: High
Force: High (Balanced)
Astrin: High and low
Force: Low (Unbalanced)
B
Astrin
Normalized signal intensity
0.12
1.00
-0.02
0.54
****
Prometa.
Meta.
Polar
Equatorial
Control
Vif
CENP-C
0.98
1.00
0.89
0.90
C
Sister KT
0.3
0.5
0.2
0.2
Metaphase
Vif
Astrin
CENP-C
D
pHec1(S55)
pS55
G
Hec1/CC/DNA
Hec1
E
Hec1 pS55
Normalized Signal Intensity
1.0
0.2
0.5
1.0
F
Sister KT (Hec1 pS55)
H
Hec1
1.0
0.8
1.0
1.1

Figure 6

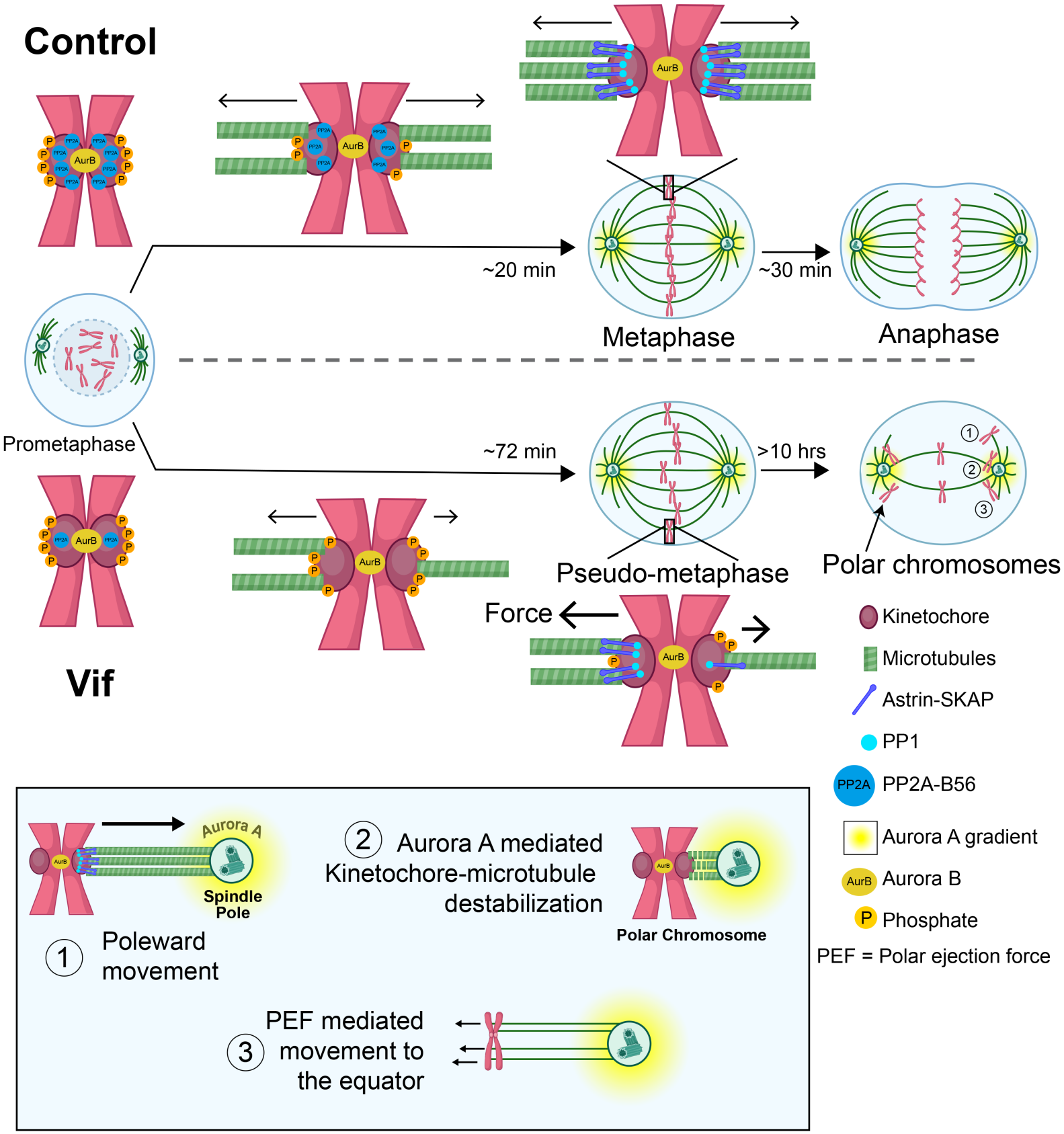
Control
AurB
PP2A
P
~20 min
~30 min
Metaphase
Anaphase
Prometaphase
~72 min
>10 hrs
Pseudo-metaphase
Polar chromosomes
Force
Vif
Kinetochore
Microtubules
Astrin-SKAP
PP1
PP2A-B56
Aurora A gradient
Aurora B
Phosphate
PEF = Polar ejection force
Aurora A
Spindle Pole
1 Poleward movement
2 Aurora A mediated Kinetochore-microtubule destabilization
Polar Chromosome
3 PEF mediated movement to the equator

Figure 7